

Article

Resilient Modulus—Physical Parameters Relationship of Improved Red Clay by Dynamic Tri-Axial Test

Haiping Yuan ¹, Weiqiang Li ¹, Yixian Wang ^{1,2,*} , Hang Lin ³  and Yan Liu ⁴

¹ School of Civil Engineering, Hefei University of Technology, Hefei 230009, China; seapie@163.com (H.Y.); lwq2015@hfut.edu.cn (W.L.)

² State Key Laboratory of Geomechanics and Geotechnical Engineering, Institute of Rock and Soil Mechanics, Chinese Academy of Sciences, Wuhan 430071, China

³ School of Resources and Safety Engineering, Central South University, Changsha 410083, China; linhangabc@126.com

⁴ State Key Laboratory of Explosion Science and Technology (Beijing Institute of Technology), Beijing 100081, China; liuyan@bit.edu.cn

* Correspondence: wangyixian2012@hfut.edu.cn

Received: 4 January 2019; Accepted: 7 March 2019; Published: 19 March 2019



Abstract: As one of the important parameters used in the analysis and design of subgrade, resilient modulus is directly related to the safety, economic and life time of subgrade structure. In this paper, the characteristics of resilient modulus of improved red clay at different additive content were studied through conducting laboratory repeated load tri-axial tests. The influence of stress state, moisture content, compactness, additive types, and content on resilient modulus were analyzed. In addition, the regression analysis of resilient modulus, was carried out referencing three existing prediction models. The results showed that the Andrei model can better fit the resilient modulus of red clay and have a higher determination coefficient. However, the Andrei model and other existing prediction models, reflect only the influence of stress state on resilient modulus, without considering the influence of moisture content, compactness and additive content. Therefore, based on the Andrei model, a comprehensive prediction model, which can reflect the influence of compactness, moisture content, additive content, and stress state on resilient modulus was introduced. Good agreement between the regression results and the measured ones demonstrated the integrative ability of the introduced model.

Keywords: red clay; additive; resilient modulus; prediction models; new comprehensive prediction model

1. Introduction

With the development of the national economy, high speed and heavy loads are inevitably the developing trend of the traffic line. In this context, static design methods will not be able to meet the increasing requirements of subgrade and pavement materials for strength and deformation. Therefore, more attention should be paid to dynamic and creep characteristics [1–8]. Soils and rocks are natural subgrade and pavement materials in the flood plain. When these are stressed, they go through stages of deformation such as elastic deformation, ductile deformation and fracture [9–20]. As a special soil, red clay is widespread in China and mainly located in the humid and rainy southern region. At present, land use is becoming more and more serious. It is the development direction and inevitable trend to make full use of the local red clay to fill the subgrade. However, the stability of the clay subgrade is particularly prominent because of the adverse factors, such as rainy weather and heavy load [21–24].

In addition, red clay should not be directly used as subgrade filling, due to the high natural moisture content and poor stability. It is necessary to include additives to improve the mechanical properties of red clay, so as to meet the filling requirements. At present, there have been some research on the mechanical properties of the improved red clay with additives, but the stability of the red clay subgrade, under dynamic loading is seldom involved [25–29].

The concept of dynamic resilient modulus of subgrade soil was introduced by Seed et al. [30], who studied the relationship between the resilient (elastic and reversible) characteristics of subgrade soil and the fatigue damage of asphalt pavement. In fact, the tensile stress and cracks, caused by the accumulation of permanent strains are the major cause of the damage of the subgrade and pavement materials [31–35]. Therefore, flexible pavement and resilient modulus values can replace compaction degree (CD) and California bearing ratio (CBR) values to reflect the stress-strain relationship of pavement structures under repeated vehicle load. A resilient modulus is one of the main parameters characterizing the mechanical properties of subgrade soils and can well-reflect the stability of subgrade soil [32]. However, it is difficult to apply and popularize a resilient modulus in practical engineering because of the test operation's complexity and high cost of tests. Therefore, it is necessary to establish models for the prediction of resilient modulus. Moreover, the prediction models can provide a reliable basis for the selection of material parameters in the structure design [36–41]. For a long time, many scholars at home and abroad have deeply explored the main factors affecting the resilient modulus of subgrade soil and established many prediction models, based on different factors, such as stress state and basic physical properties of soil [42–47]. According to the different stress variables, prediction models can be divided into three categories: Single factor model related to mass stress, a composite model related to shear stress and mass stress, and a composite model related to shear stress and confining pressure [48–60]. However, most of existing prediction models only consider the influence of stress state on the resilient modulus [42], and rarely consider the influence of compactness, moisture content, and additive content. They are generally linear fitting [35–38], or combine a single physical parameter to predict the resilient modulus [43,44].

In the design of subgrade structure, the resilient modulus is different, according to the subgrade grade. In this paper, the red clay in Anhui, China was chosen to be improved by two types of additives. Through laboratory repeated load tri-axial tests, the influence of stress state, moisture content, compactness, additive type, and content on resilient modulus were analyzed. According to the research experience [61–66], based on existing prediction models, which fail to incorporate the influence of moisture content, compactness and additive content, a comprehensive prediction model which can reflect the influence of compactness, moisture content, additive content and stress state on resilient modulus was introduced. To conclude the performance of the introduced model, the predicted and the measured resilient modulus were paralleled. The parallel found the introduced model capable of capturing the characteristics of the measured resilient modulus [54]. By comparison and verification, it was found that the proposed model predicts the modulus of resilience of the improved clay with additives of various contents, indicating that it has some potential in engineering applications.

2. Material Properties and Testing Method

2.1. Materials

The basic properties of the red clay used in the test are shown in Table 1. In order to analyze the influence of stress state, moisture content, compactness, additive type and content on the resilient modulus of red clay, samples prepared at different moisture content (OMC minus 3%, OMC, OMC plus 3%), different compactness of P (91%, 93%, 95%), different additive types (ordinary Portland cement, lime) and content (3%, 6%, 9%) were tested.

Table 1. Basic properties of red clay.

Samples	Grain Density	Natural Dry Density	Maximum Dry Density	Optimum Moisture Content	Liquid Limit	Plastic Limit	<0.075mm Grain Size
	/(g/cm)	/(g/cm)	/(g/cm)	/%	/%	/%	Soil particle content/%
Red clay	2.72	1.28	1.73	27.8	52.6	30.7	90

The chemical and mineral compositions of the red clay, obtained from X-ray diffraction measurements, are summarized in Table 2, and Table 3, respectively. It is indicated that the mineral compositions include mainly kaolinite (i.e., $\text{Al}_2\text{Si}_2\text{O}_5(\text{OH})_4$), goethite (i.e., $\text{FeO}(\text{OH})$), and diasporite (i.e., SiO_2). The amount of kaolinite is 60.87%. Therefore, kaolinite dominates the mineral compositions of the red clay.

Table 2. Chemical compositions of red clay.

Constituents	SiO_2	Al_2O_3	Fe_2O_3	K_2O	MgO	CaO	Na_2O	LOI
Content(%)	40.27	32.65	18.52	2.51	0.91	0.72	0.24	4.18

Table 3. Mineral composition of red clay.

Mineral	Mineral Compositions/(%)				
	$\text{Al}_2\text{Si}_2\text{O}_5(\text{OH})_4$	$\text{Al}(\text{OH})_3$	$\text{FeO}(\text{OH})$	SiO_2	Deviation
Content(%)	60.87	11.72	13.13	11.96	-2.32

Proctor compaction tests were carried out to determine maximum dry densities and optimum moisture contents of the improved red clay samples which are presented in Table 4. Based on the compaction test results, the samples were prepared at the targeted compactness and moisture content.

Table 4. Proctor compaction test results on samples with different additive contents.

Cement Content/%	Optimum Moisture Content/%	Maximum Dry Density/(g/cm ³)	Lime Content/%	Optimum Moisture Content/%	Maximum Dry Density/(g/cm ³)
3	25.6	1.75	3	26.2	1.74
6	24.3	1.76	6	25.1	1.75
9	23.2	1.78	9	24.2	1.76

The samples were prepared according to China highway geotechnical test code (JTGE40-2007). The samples were prepared as follows: Drying, grinding, mixing with additive, curing, and preparation. Three parallel samples were prepared for each group with different admixtures. The samples were placed in a standard curing room with $25 \pm 2^\circ\text{C}$ for 7 days. For each sample, the difference between the actual and the targeted moisture contents is less than 1%, and that difference is less than 2% for compactness.

2.2. Testing Method

In the test, the resilient modulus values were measured by the dynamic servo system UTM400. The loading waveform is half-sine waveform and the load frequency is 1 Hz. The holding time and interval time are 0.1 s, and 0.9 s, respectively. The repeated load and resilient strain were measured by load sensor and displacement sensor respectively in the dynamic tri-axial chamber. The adopted stress loading sequence of subgrade soil was obtained from the international research results [67–70]. It is necessary to preload the samples before the test to simulate the history of subgrade stress during construction, eliminate the influence of load difference factors, such as initial loading and repeated loading and reduce the variability of test results. In addition, preloading can eliminate the possible bad contact between the bottom of the samples and the pressure plate to improve the accuracy of the

test [70]. A dynamic resilient modulus is defined as the ratio of repeated axial deviatoric stress to the recoverable axial strain as Figure 1. The cyclic number of loading is 100, and the average resilient deformation during the last 5 cycles, for each magnitude of repeated loading, was recorded. The dynamic resilient modulus of samples was calculated according to Equation (1).

$$M_r = \frac{\Delta\sigma_d}{\Delta\varepsilon_{axial}} \tag{1}$$

where $\Delta\sigma_d$ = deviatoric stress ($= \sigma_1 - \sigma_3$), σ_1 and σ_3 = major and minor principal stresses, and $\Delta\varepsilon_{axial}$ = recoverable axial strain.

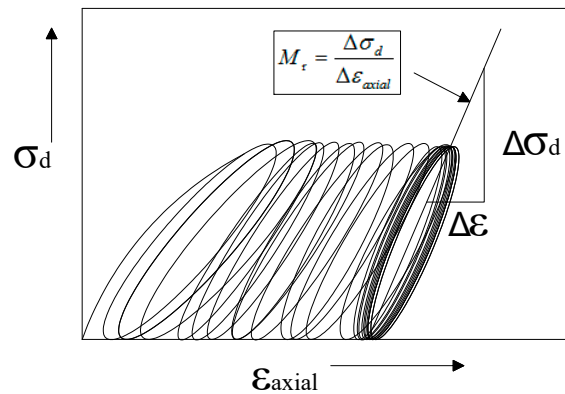


Figure 1. Definition of dynamic resilient modulus (Hopkins et al., 2001 [51]).

3. Analysis of Results

3.1. Influence of Stress State on Resilient Modulus

Figure 2 shows the variation of resilient modulus with deviatoric stress and bulk stress of the improved red clay. It can be seen from Figure 2 that for the improved red clay, when the confining pressure is constant, the resilient modulus decreases with an increase in deviatoric stress; when the deviatoric stress is constant, the resilient modulus increases with an increase in confining pressure. At the same time, in the repeated load triaxial test, $\sigma_2 = \sigma_3 =$ confining pressure, $3\sigma_3 + \sigma_d =$ bulk stress, octahedral shear stress is $\tau_{oct} = \sqrt{2}\sigma_d/3$. Therefore, the effects of confining pressure and deviatoric stress on the resilient modulus need to be discussed. The results of the two-factor variance analysis of resilient modulus of the improved red clay, with 3% cementor 3% lime, are presented in Table 5. It can be seen from Table 5 that the effects of confining pressure and deviatoric stress on the resilient modulus are remarkable.

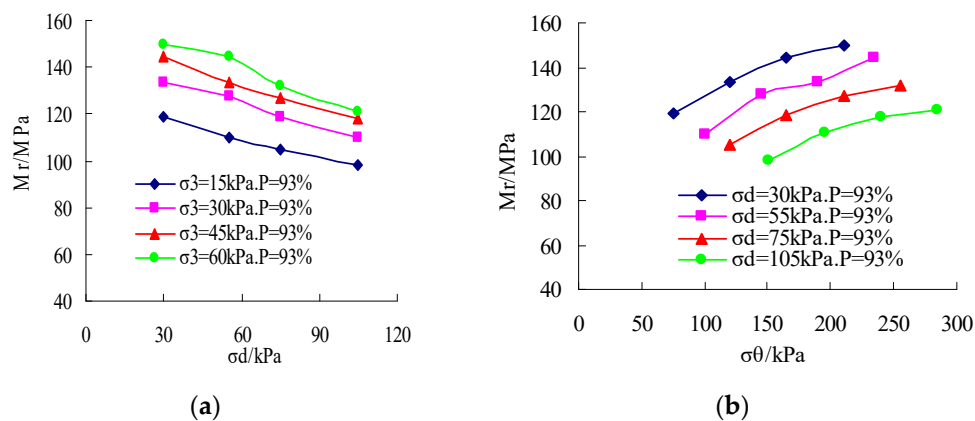


Figure 2. Cont.

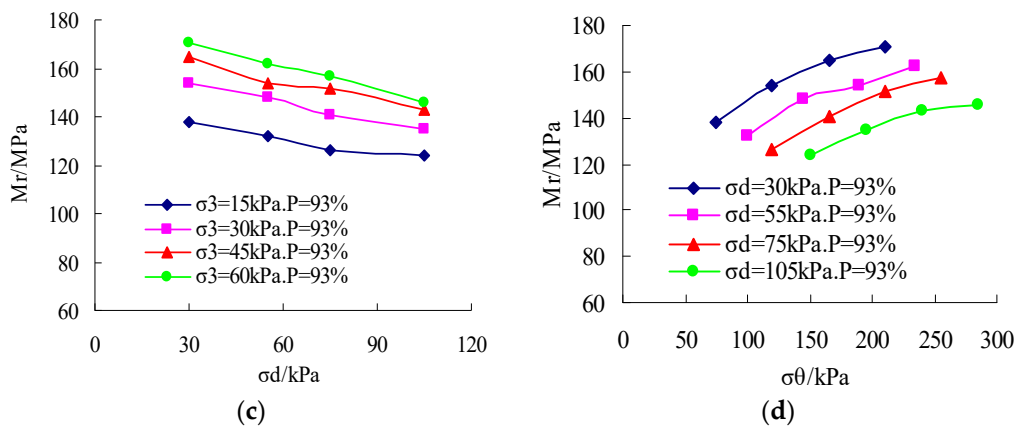


Figure 2. Variation of resilient modulus with deviatoric stress and bulk stress. (a) Lime 3% OMC $M_r - \sigma_d$; (b) Lime 3% OMC $M_r - \sigma_\theta$; (c) Cement 3% OMC $M_r - \sigma_d$; (d) Cement 3% OMC $M_r - \sigma_\theta$.

Table 5. Two-factor variance analysis of resilient modulus.

(a) Improved red clay with 3% cement						
Source of Variation	Variance Sum	Degree of Freedom	Mean Square Error	F Value	Critical Value $\alpha = 0.05$	Significance
Deviatoric stress	2397.41	3	799.136	134.39	3.86	Significant
Confining pressure	1832.63	3	610.877	102.73	3.86	Significant
Error	53.52	9	5.946			
Sum	4283.56	15				
(b) Improved red clay with 3% lime						
Source of Variation	Variance Sum	Degree of Freedom	Mean Square Error	F Value	Critical Value $\alpha = 0.05$	Significance
Deviatoric stress	1853.83	3	617.942	178.36	3.86	Significant
Confining pressure	1870.63	3	623.544	179.98	3.86	Significant
Error	31.18	9	3.465			
Sum	3755.64	15				

3.2. Prediction Models of Resilient Modulus

The concept of a resilient modulus has been used to represent the non-linear stress-strain characteristics of subgrade soils. From the above analysis, it can be concluded that the resilient modulus of improved red clay has a strong dependence on the stress state. Several prediction models have been developed in the past to express the relationship between resilient modulus and stress state. The prediction models of non-linear resilient modulus mainly include the single factor model related to bulk stress or deviatoric stress [36], the composite model related to deviatoric stress, and mass stress [38], the composite model related to shear stress and confining pressure [40], and the composite model related to confining pressure and deviatoric stress [41]. In this paper, three prediction models frequently cited were chosen to analyze the influence of deviatoric stress and confining pressure on the resilient modulus of the improved red clay.

3.2.1. Uzan-Witczak Model

Uzan-witczak [38] introduced deviatoric stress and bulk stress to characterize the influence of stress state on the resilient modulus, and established the nonlinear constitutive model, as shown in Equation (2).

$$M_R = k_1 \theta^{k_2} \sigma_d^{k_3} \tag{2}$$

where σ_d is the deviatoric stress and k_1, k_2 and k_3 are regression coefficients.

θ is the bulk stress that is given as

$$\theta = \sigma_1 + \sigma_2 + \sigma_3$$

where σ_1 is the major principal stress; σ_2 is the intermediate principal stress, and σ_3 is the minor principal stress or confining pressure (= σ_2 for M_R test in triaxial test)

However, this prediction model has some limitations: when σ_d equals 0, the result of Equation (2) tends to infinity. When σ_1 and σ_3 equal 0, the result is $0 \cdot \infty$.

3.2.2. Andrei Model

In the practical problem, the intermediate and the minor principal stresses are not equal. In order to consider the influence of both of them on the resilient modulus, Andrei model [40] introduced the octahedral shear stress to replace the deviatoric stress in the May and Witczak model [71]. This operation provides a better explanation of the stress state of the materials, and further generalize the nonlinear constitutive model, as shown in Equation (3).

$$M_R = k_1 P_a \left(\frac{\theta}{P_a} \right)^{k_2} \left(\frac{\tau_{oct}}{P_a} + 1 \right)^{k_3} \tag{3}$$

where τ_{oct} is the octahedral shear stress, P_a = atmospheric pressure and k_1, k_2 and k_3 are regression coefficients.

θ is the mass stress that is given as

$$\theta = \sigma_1 + \sigma_2 + \sigma_3$$

τ_{oct} is given as

$$\tau_{oct} = \frac{1}{3} \sqrt{(\sigma_1 - \sigma_3)^2 + (\sigma_1 - \sigma_2)^2 + (\sigma_2 - \sigma_3)^2}$$

where σ_1 is the major principal stress; σ_2 is the intermediate principal stress and σ_3 is the minor principal stress or confining pressure.

In this prediction model, the influence of bulk stress and octahedral shear stress on the resilient modulus was fully taken into account. Compared with Equation (2), the Andrei model is essentially consistent with the Uzan-Witczak model. The difference between them is that the term $\frac{\tau_{oct}}{P_a}$ in the Andrei model is followed by an additional constant of 1, eliminating the existing problems of the Uzan-Witczak model.

3.2.3. Ni Model

Based on testing results, Ni et al. [41] found that the resilient modulus was very sensitive to confining pressure, because of this, they introduced confining pressure and deviatoric stress to the prediction model to eliminate the existing problems included in the above Uzan-Witczak model. The following prediction model was given (Equation (4)):

$$M_R = k_1 P_a \left(\frac{\sigma_3}{P_a} + 1 \right)^{k_2} \left(\frac{\sigma_d}{P_a} + 1 \right)^{k_3} \tag{4}$$

where σ_3 is the minor principal stress or confining pressure, σ_d is the deviatoric stress, P_a = atmospheric pressure, and k_1, k_2 and k_3 are regression coefficients.

Due to the difference in the physical properties of red clay in different regions, the selected prediction models were different from each other. In this paper, the above-mentioned prediction models of the resilient modulus were selected for red clay in Anhui province.

3.3. Regression Analysis Results

The fitting performance of a regression model is frequently evaluated by the determination coefficient, R^2 , defined as the ratio of regression sum of squares (SSR) to total sum of square (SST), that is $R^2 = SSR/SST$.

$$SSR = \sum_{i=1}^n (y_i - \hat{y}_i)^2 \quad (5)$$

$$SST = \sum_{i=1}^n (y_i - \bar{y}_i)^2 \quad (6)$$

In Equations (5) and (6), y_i is actual value, \hat{y}_i is predicted value, \bar{y}_i is sample mean, SSR is regression sum of squares, SST is total sum of square.

Regression analysis of the test data was conducted for various conditions, and the results are shown in Table 6. From the regression results, a high coefficient of determination between the three prediction models, and the test results, is observed. For the Uzan-Witczak model, NI model and Andrei model, the coefficient of determination R^2 was greater than 0.80, 0.934, and 0.937, respectively. By comparing the coefficients of determination for the three prediction models, it can be concluded that the regression results, generated by the Andrei model and the NI model, are better than the regression results generated by the Uzan-Witczak model. In particular, the Andrei model can fit the test data better than the NI model does.

In the above three prediction models of the resilient modulus, k_1 is used to characterize the stiffness of the subgrade soil and is proportional to the resilient modulus. The value of k_1 increases with an increase in effective stress, additive content and compactness, and decreases with an increase in moisture content. k_2 reflects the influence of confining pressure (bulk stress) on resilient modulus and is positively associated with confining pressure. The value of k_2 as a whole decreases with an increase in moisture content, and increases with an increase in additive content and compactness. The value of k_3 is negative, indicating that a negative correlation between the resilient modulus and the deviatoric stress (octahedral shear stress). k_3 shows that the dynamic resilient modulus of subgrade soils decreases with an increase in shear stress, and its value is not obviously related to the moisture content and the compactness.

Table 6. Parameters required in different prediction models of resilient modulus.

Additive Content	Compactness/%	Moisture Content/%	Uzan-Witczak Model				NI Model				Andrei Model			
			k1	k2	k3	R2	k1	k2	k3	R2	k1	k2	k3	R2
C6%	93	OMC minus 3%	139.6	0.2047	-0.2176	0.9260	1791.6	0.5045	-0.3637	0.9556	2033.8	0.1974	-0.9476	0.9618
		OMC	148.88	0.1953	-0.2225	0.9146	1733	0.5054	-0.4431	0.9421	1960.5	0.1999	-1.0855	0.9569
		OMC plus 3%	152.38	0.1083	-0.1391	0.9191	1585	0.2844	-0.2882	0.9669	1697.6	0.1116	-0.6782	0.9739
L6%		OMC minus 3%	123.97	0.2168	-0.2198	0.9375	1578.1	0.5632	-0.4147	0.9718	1816.1	0.2214	-1.0717	0.9812
		OMC	149.13	0.1901	-0.2585	0.934	1513	0.5253	-0.5224	0.9782	1716.3	0.2016	-1.2226	0.9721
		OMC minus 3%	129.48	0.1445	-0.1667	0.9182	1439.2	0.3776	-0.3333	0.9662	1579.2	0.1489	-0.8169	0.9788
C6%	91	OMC	155.61	0.1811	-0.2402	0.8621	1667.8	0.4873	-0.5172	0.9342	1874.8	0.189	-1.1987	0.9434
	93		148.88	0.1953	-0.2225	0.9146	1733	0.5054	-0.4431	0.9421	1960.5	0.1999	-1.0855	0.9569
	95		165.93	0.198	-0.2418	0.8084	1851.3	0.5399	-0.5119	0.9005	2112.9	0.2086	-1.2227	0.909
L6%	91	OMC	115.10	0.2107	-0.2136	0.9266	1446.8	0.557	-0.3953	0.962	1664	0.2123	-1.0225	0.9374
	93		149.13	0.1901	-0.2585	0.934	1513	0.5253	-0.5224	0.9782	1716.3	0.2016	-1.2226	0.9721
	95		144.19	0.2147	-0.244	0.8937	1708	0.5644	-0.4923	0.945	1961.7	0.2216	-1.2071	0.96
C3%	93	OMC	94.43	0.2335	-0.1859	0.9596	1405	0.5954	-0.2959	0.9664	1637.3	0.236	-0.8898	0.9753
C6%			148.88	0.1953	-0.2225	0.9146	1733	0.5054	-0.4431	0.9421	1960.5	0.1999	-1.0855	0.9569
C9%			107.73	0.2577	-0.2073	0.9224	1655.5	0.6738	-0.3373	0.9656	1969.8	0.2615	-1.0027	0.9514
L3%			86.24	0.2671	-0.2462	0.9399	1241.3	0.6923	-0.4427	0.9681	1477.3	0.2719	-1.1974	0.974
L6%			149.13	0.1901	-0.2585	0.934	1513	0.5253	-0.5224	0.9782	1716.3	0.2016	-1.2226	0.9721
L9%			155.61	0.1885	-0.2449	0.9156	1658.2	0.4997	-0.5133	0.9545	1868.9	0.1928	-1.1943	0.9543

Table 7 and Figure 3 show that predicted resilient modulus versus measured resilient modulus for the improved red clay prepared at 93% compactness and 6% additive (cement and lime). It can be seen that the maximum errors, between the measured and the predicted resilient modulus, by using the Andrei model, NI model and Uzan-Witczak model are, respectively, 4.533%, 3.934%, and 6.133%. In addition, the average error and variance of Andrei, NI and Uzan-Witczak models are $1.70\% \pm 1.14\%$, $2.11\% \pm 1.07\%$, and $2.32\% \pm 1.75\%$, respectively. It can be concluded that the fitting performance of Andrei model is better than that of NI model and Uzan-Witczak model.

Table 7. Test data and forecast data of different prediction models.

Mass Stress σ/kPa	Octahedral Shear Stress/kPa	Measured Data/Mpa	Resilient Modulus					
			Andrei Model		NI Model		Uzan-Witczak Model	
			Predicted Value/Mpa	Error/%	Predicted Value/Mpa	Error/%	Predicted Value/Mpa	Error/%
75	14.14	160	160.3371	0.2102	165.572	3.3653	162.302	1.4184
100	25.93	150	152.6465	1.7338	153.1579	2.0618	150.0214	0.0143
120	35.36	144	146.379	1.6252	145.1393	0.785	145.0932	0.7534
150	49.5	132	137.405	3.9336	135.3122	2.4479	140.6242	6.1328
120	14.14	180	176.1317	2.1962	176.1559	2.1822	177.9052	1.1775
145	25.93	167.4	164.4161	1.8148	162.9482	2.732	161.3126	3.7736
165	35.36	158	156.0003	1.2819	154.4171	2.3203	154.4036	2.3292
195	49.5	145.9	144.8037	0.7571	143.9618	1.3463	148.0175	1.4306
165	14.14	187	187.7086	0.3775	186.1511	0.456	189.3211	1.226
190	25.93	180	173.5441	3.7201	172.194	4.5333	170.0567	5.847
210	35.36	165.3	163.705	0.9743	163.1788	1.2999	161.8498	2.1317
240	49.5	153.5	150.9406	1.6956	152.1303	0.9003	154.1433	0.4173
210	14.14	190.5	196.9794	3.2894	195.6467	2.6306	198.4513	4.0067
235	25.93	182.7	181.077	0.8963	180.9776	0.9517	177.2649	3.0661
255	35.36	166	170.1836	2.4583	171.5026	3.2084	168.1048	1.2521
285	49.5	155.9	156.2159	0.2022	159.8905	2.4958	159.4045	2.1985

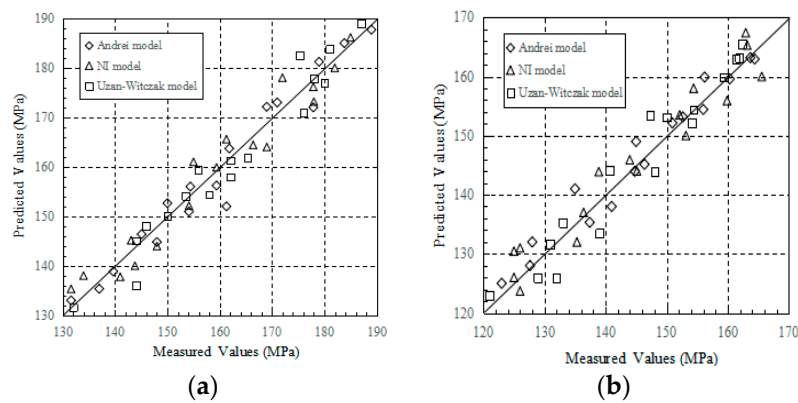


Figure 3. Predicted resilient modulus versus measured resilient modulus by three prediction models (Andrei model, NI model and Uzan-Witczak model). (a) 93% compactness and 6% cement; (b) 93% compactness and 6% lime.

4. The Dependence of Resilient Modulus on Material Properties

4.1. The Influence of Moisture Content and Compactness on Resilient Modulus

The improved red clay samples, prepared at 93% compactness and 6% cement (C6%), and prepared at 93% compactness and 6% lime (L6%), were selected to study the influence of different moisture content on the dynamic resilient modulus of the improved red clay. As can be seen from Figure 4, the resilient modulus of the improved red clay is greatly affected by moisture content, and its value decreases with an increase in moisture content. For the improved red clay with 6% cement, when the confining pressure is 15 kPa and the deviatoric stress is 30 kPa, the resilient modulus for the optimum moisture content (OMC) of 21.5% (OMC minus 3%), 24.3% (OMC), 27.1% (OMC plus 3%) is

171.2 MPa, 158.0 MPa, 147.7 MPa, respectively. Compared with the moisture content of 21.5% (OMC minus 3%), the resilient modulus for moisture content of 24.3%, and 27.1% (OMC plus 3%) decreases by 7.71%, and 14.1%, respectively. In addition, when the moisture content is invariable, the resilient modulus of improved red clay decreases with an increase in deviatoric stress, and increases with an increase in mass stress.

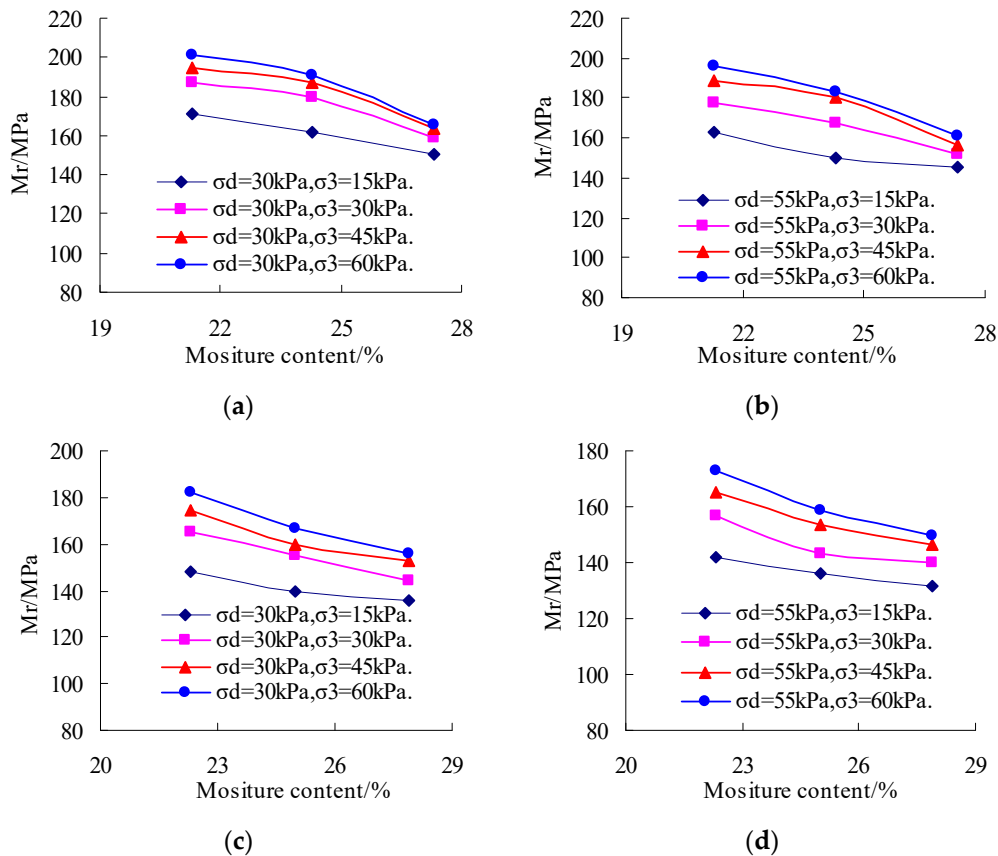


Figure 4. $M_R - w$ relation curve at different stress states. (a) $C6\%$, $P93\%$, $\sigma_d = 30$ kPa; (b) $C6\%$, $P93\%$, $\sigma_d = 55$ kPa; (c) $L6\%$, OMC , $\sigma_d = 30$ kPa; (d) $L6\%$, $P93\%$, $\sigma_d = 55$ kPa.

The improved red clay samples, prepared at optimum moisture content and 6% cement, and prepared at OMC and 6% lime ($L6\%$), were selected to study the influence of different compactness on the dynamic resilient modulus. As can be seen from Figure 5, when the moisture content is invariable, the resilient modulus of the improved red clay increases with an increase in compactness. For the improved red clay with 6% cement, when the confining pressure is 60 kPa and the deviatoric stress is 30 kPa, the resilient modulus for the red clay samples, when prepared at a compactness of 91%, 93%, and 95% is 177.89 MPa, 190.5 MPa, and 204.67 kPa, respectively. Compared with 91% compactness, the resilient modulus for compactness of 93%, and 95% increases by 7.08%, and 15.05%, respectively. In addition, when the compactness is invariable, the resilient modulus of the improved red clay decreases with an increase in deviatoric stress and increases with an increase in bulk stress.

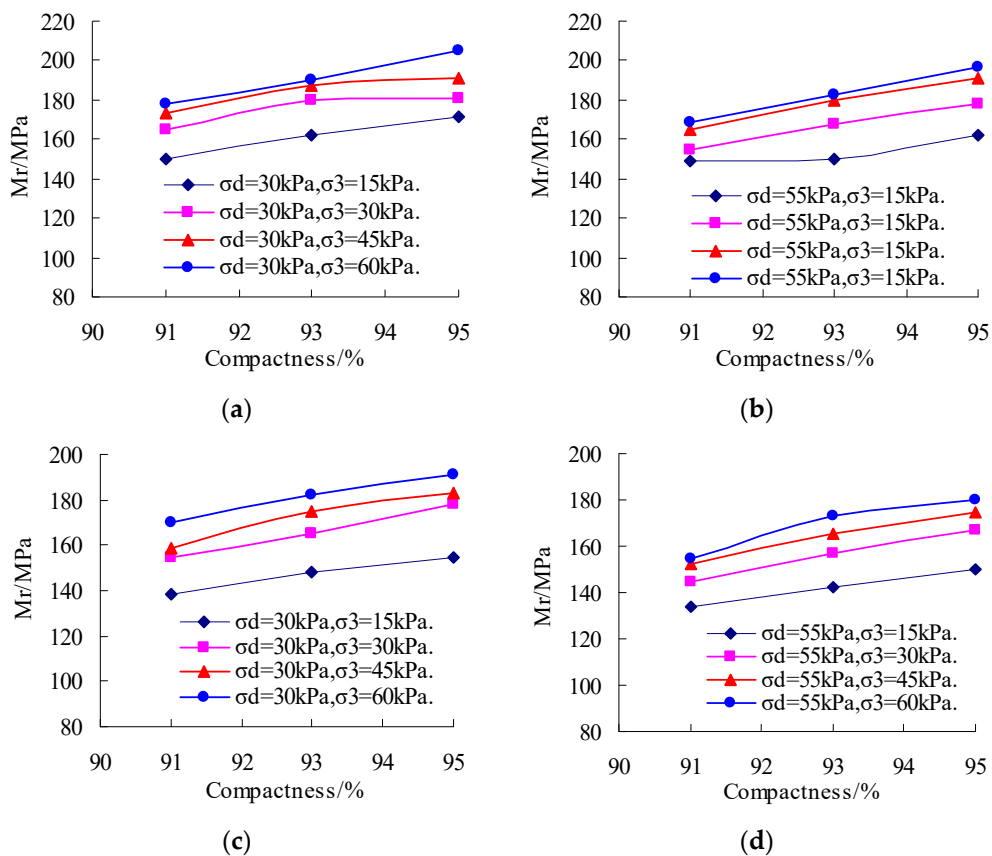


Figure 5. $M_R - P$ curve at different stress states. (a) $C6\%$, OMC , $\sigma_d = 30$ kPa; (b) $C6\%$, OMC , $\sigma_d = 55$ kPa; (c) $L6\%$, OMC , $\sigma_d = 30$ kPa; (d) $L6\%$, OMC , $\sigma_d = 55$ kPa.

4.2. The Influence of Additive Content on Resilient Modulus

The improved red clay prepared at optimum moisture content and 93% compactness were selected to study the influence of different additives on the dynamic resilient modulus of the improved red clay. As can be seen from Figures 6 and 7, both cement and lime (3–9%) can significantly improve the dynamic resilient modulus of the red clay. In Figure 6, when the confining pressure is 60 kPa and the deviatoric stress is 30 kPa, the resilient modulus of red clay samples, prepared at a lime content of 3%, 6%, and 9% is 149.9 MPa, 166 MPa, and 180.6 MPa, respectively. Compared with 3% lime, the resilient modulus for lime content of 6%, 9% increases by 10.75%, and 20.4%, respectively. In Figure 7, when the confining pressure is 60 kPa and the deviatoric stress is 30 kPa, the resilient modulus of red clay with cement content of 3%, 6%, and 9% is 170.4 MPa, 190.5 MPa, and 202 MPa, respectively. Compared with 3% cement, the resilient modulus for cement content of 6%, and 9% increases by 11.8%, and 18.54%, respectively. By comparing Figure 6a with Figure 7a, it can be concluded that when the confining pressure is 60 kPa and the deviatoric stress is 30 kPa, an increase of 12% in the dynamic resilient modulus was observed for 3% cement, compared with that of 3% lime. By comparing other data, it can be also seen that, when the contents of cement and lime are the same, cement can significantly improve the resilient modulus of red clay.

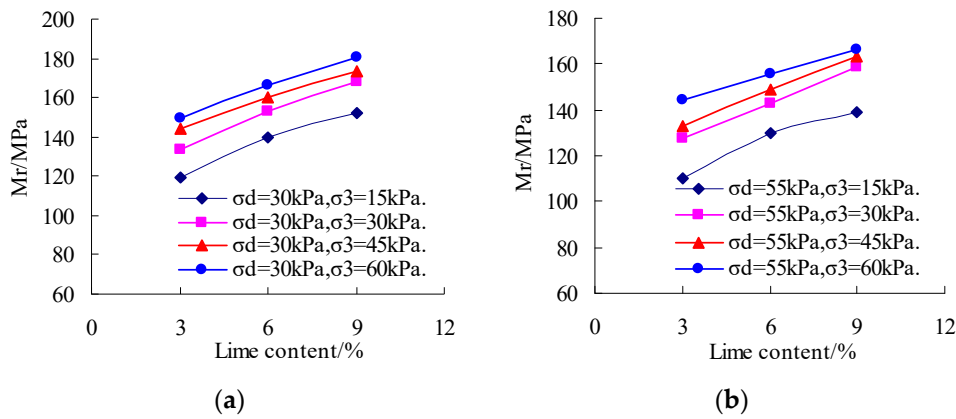


Figure 6. Relationship between resilient modulus (M_r) and lime content for various stress states. (a) OMC, P93%, $\sigma_d = 30$ kPa; (b) OMC, P93%, $\sigma_d = 55$ kPa.

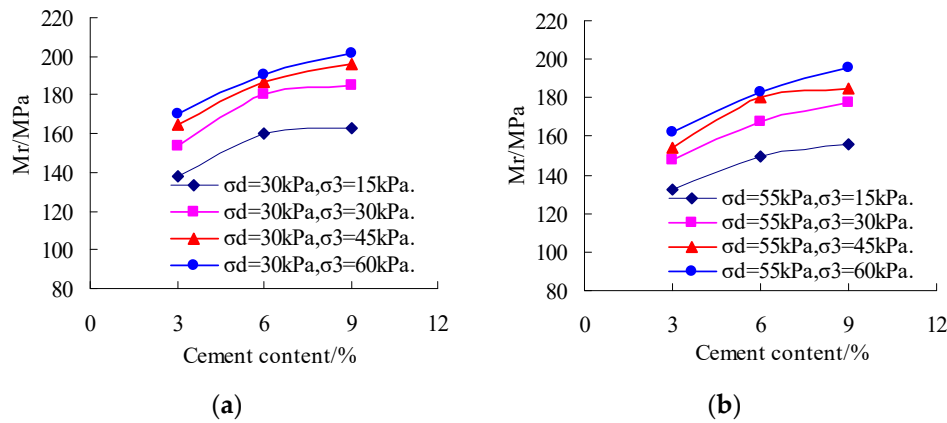


Figure 7. Relationship between resilient modulus (M_r) and cement content for various stress states. (a) OMC, P93%, $\sigma_d = 30$ kPa; (b) OMC, P93%, $\sigma_d = 55$ kPa.

4.3. New Comprehensive Prediction Model

From the analysis of the existing prediction models, it can be concluded that the Andrei model can better predict the resilient modulus of the red clay chosen for this test. However, the Andrei model and other existing prediction models reflect only the influence of the stress state on resilient modulus, but the influence of moisture content, compactness, and additive content were not considered. Lu et al. proposed a new methodology to convert the band shaped drain into an annular instead of a circle to keep the sectional area or perimeter of the band shaped drain unchanged before and after the conversion [72]. From Figure 4 through 7, it can be seen that the resilient modulus is correlated negatively with moisture content, meaning that the higher the moisture content, the smaller the resilient modulus. Additionally, the resilient modulus is correlated positively with the compactness and the additive content, which means that the greater the compactness and the additive content, the larger the resilient modulus. It can be concluded that the influence of compactness, moisture content, and additive content on the resilient modulus is remarkable.

In this paper, considering the above factors affecting the resilient modulus, the relationship between moisture content (W), compactness (P), additive content (C), octahedral shear stress (τ_{oct}), bulk stress (θ), atmospheric pressure (P_a) and resilient modulus (M_R) are established, which is expressed as a Equation (7).

$$F(W, P, C, \tau_{oct}, \theta, P_a, M_R) = 0 \tag{7}$$

As the resilient modulus is correlated positively with the compactness and the additive content, and negatively with the moisture content, based on dimensional analysis [73], Equation (7) can be transformed into Equation (8).

$$F(P/W, C/W, \tau_{oct}/P_a, \theta/P_a, M_R) = 0 \tag{8}$$

On this basis, combined with the above existing prediction models, to eliminate the influence of dimension, the compactness and the additive content were normalized by the moisture content, respectively. The following prediction model was given (Equation (9)). In Equation (9), to eliminate the problem that the predicted value of resilient modulus is 0, $\frac{C}{W}$ and $\frac{\tau_{oct}}{P_a}$ add 1, respectively.

$$M_R = k_1 P_a \left(\frac{P}{W}\right)^{k_2} \left(\frac{C}{W} + 1\right)^{k_3} \left(\frac{\theta}{P_a}\right)^{k_4} \left(\frac{\tau_{oct}}{P_a} + 1\right)^{k_5} \tag{9}$$

where τ_{oct} is the octahedral shear stress, P_a = atmospheric pressure, k_1, k_2, k_3, k_4 and k_5 are regression coefficients, θ is the bulk stress, P is compactness, C is additive content, W is moisture content, and P_a is atmospheric pressure.

Regression analysis of the testing results on the red clay samples improved with cement and/or lime was carried out by using Equation (9). Presented in Table 8 are the parameters that the proposed prediction model requires, the determination coefficient of improved red clay samples prepared at different moisture content, and the compactness and additive content. For prediction models, the greater the determination coefficient, R^2 , the better the regression effect, indicating a higher rationality and reliability of the prediction model. The determination coefficient of the proposed comprehensive prediction model for the additive of cement and lime is 0.84, and 0.86, respectively.

Table 8. Comprehensive prediction model regression equation for two additives.

Additive	Comprehensive Prediction Model Regression Equation	R ²
Cement	$M_R = 0.6896P_a \left(\frac{P}{W}\right)^{0.5197} \left(\frac{C}{W} + 1\right)^{1.2702} \left(\frac{\theta}{P_a}\right)^{0.2042} \left(\frac{\tau_{oct}}{P_a} + 1\right)^{-0.9383}$	0.84
Lime	$M_R = 0.8096P_a \left(\frac{P}{W}\right)^{0.4186} \left(\frac{C}{W} + 1\right)^{0.9594} \left(\frac{\theta}{P_a}\right)^{0.2191} \left(\frac{\tau_{oct}}{P_a} + 1\right)^{-1.1321}$	0.86

The comparison between the predicted and the measured values are presented in Figures 8 and 9. As shown in Figures 8 and 9, the maximum error between the predicted and the testing results for different cement and lime contents is 8.67%, and 8.70%, respectively. In addition, the average error and variance of the new comprehensive prediction model for different cement and lime contents are, respectively, $3.18\% \pm 4.03\%$, and $3.06\% \pm 3.94\%$. The new comprehensive prediction model, which reflects the influence of compactness, moisture content, additive content, and stress state on resilient modulus has good regression performance.

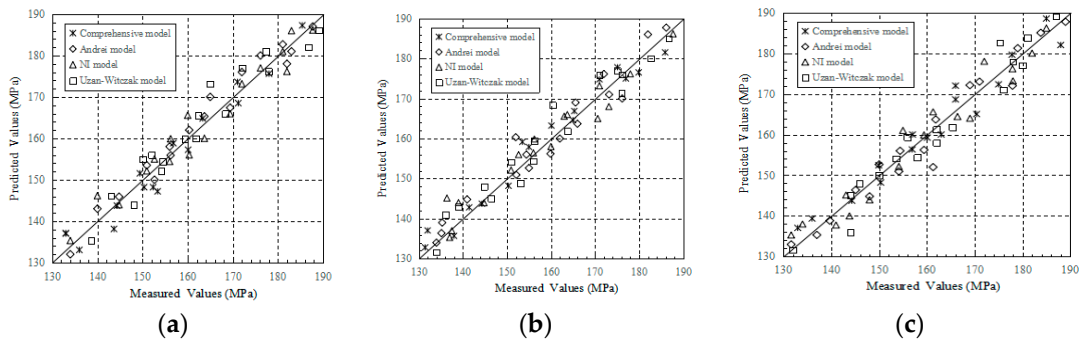


Figure 8. Predicted resilient modulus versus measured resilient modulus at different optimum moisture content, compactness and cement by four prediction models (comprehensive model, Andrei model, NI model & Uzan-Witczak model). (a) 93% compactness and 6% cement; (b) optimum moisture content (OMC) and 6% cement; (c) 93% compactness and OMC.

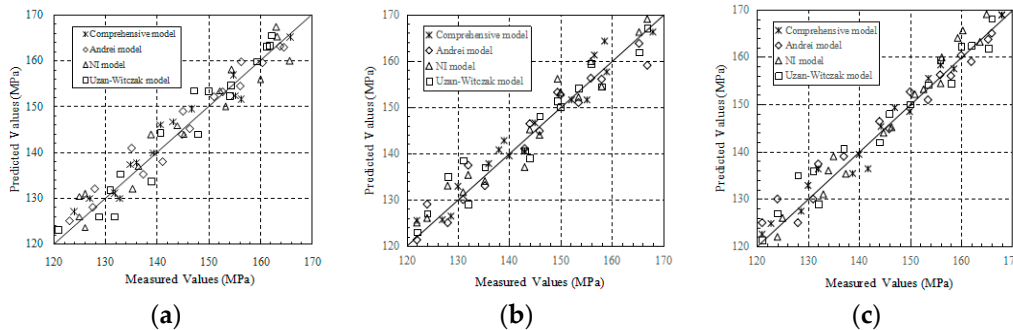


Figure 9. Predicted resilient modulus versus measured resilient modulus at different optimum moisture content, compactness and lime by four prediction models (Comprehensive model, Andrei model, NI model and Uzan-Witczak model). (a) 93% compactness and 6% lime; (b) OMC and 6% lime; (c) 93% compactness and OMC.

5. Conclusions

Due to the great difference in the physical properties of red clay in different regions, it is necessary to point out that the above predicted results are only applicable to the prediction of resilient modulus and improvement of red clay in Anhui province.

1. The testing results showed that the dynamic resilient modulus of red clay can be obviously increased by adding cement or lime (3–9%). In addition, the dynamic resilient modulus increases with an increase in compactness and additive content, and decreases with an increase in moisture content. Testing results also showed that, when the contents of cement and lime in red clay samples were the same, the dynamic resilient modulus of red clay improved with cement was slightly higher compared to that improved with lime.

2. Through a variance analysis of stress state, it can be concluded that the influence of deviatoric stress, and bulk stress on dynamic resilient modulus are significant, but the influence of deviatoric stress are more obvious. The dynamic resilient modulus of red clay increases with an increase in confining pressure. In addition, it decreases with an increase in deviatoric stress when the confining pressure is invariable, and increases with an increase in bulk stress when the deviatoric stress is invariable.

3. Three existing prediction models were used to predict the resilient modulus of the improved red clay. A comparison of the predicted results, using these prediction models, indicated that the fitting performance of the Andrei model was the best. The resilient modulus is not only affected by the stress state, but also by the compactness, moisture content, and additive content. Therefore, based on the Andrei models, a new comprehensive prediction model was proposed to reflect the influence of compactness, moisture content, additive content and stress state on resilient modulus.

By comparing the regression values with the measured values, it can be concluded that the new comprehensive prediction model has a good regression performance. The good performance applies to various additive contents, demonstrating a good potential of engineering application for the proposed prediction model.

Author Contributions: H.Y. and Y.W. conceived and designed the experiments; W.L. performed the experiments; H.L. and Y.L. analyzed the data; W.L. wrote the paper.

Acknowledgments: This research was funded by the National Natural Science Foundation of China (51874112;51774107), the Open Research Fund of State Key Laboratory of Geo-mechanics and Geotechnical Engineering, Institute of Rock and Soil Mechanics, Chinese Academy of Sciences (Z013010), the Opening Project of State Key Laboratory of Explosion Science and Technology, Beijing Institute of Technology (No. KFJJ19-02M). All financial support is gratefully acknowledged.

Conflicts of Interest: The authors declare no conflict of interest.

References

- Li, Z.Y.; Dong, C.; Zou, J.R.; Zou, W.L. Research on experiment and prediction model of dynamic resilient modulus of laterite soil in Southern Hunan. *Rock Soil Mech.* **2015**, *36*, 1840–1846.
- Wang, Y.X.; Lin, H.; Zhao, Y.L.; Li, X.; Guo, P.P.; Liu, Y. Analysis of fracturing characteristics of unconfined rock plate under edge on impact loading. *Eur. J. Environ. Civ. Eng.* **2019**. [[CrossRef](#)]
- Wu, F.; Chen, J.; Zou, Q.L. A nonlinear creep damage model for salt rock. *Int. J. Damage Mech.* **2018**, 1–14. [[CrossRef](#)]
- Zhao, Y.L.; Zhang, L.Y.; Wang, W.J.; Wan, W.; Ma, W.H. Separation of elastoviscoplastic strains of rock and a nonlinear creep model. *Int. J. Geomech.* **2018**, 04017129. [[CrossRef](#)]
- Zhao, Y.L.; Zhang, L.Y.; Wang, W.J.; Wan, W.; Li, S.Q.; Ma, W.H.; Wang, Y.X. Creep behavior of intact and cracked limestone under multi-level loading and unloading cycles. *Rock Mech. Rock Eng.* **2017**, *50*, 1409–1424. [[CrossRef](#)]
- Qiu, X.; Yang, Q.; Wang, B.R.; Luo, X.H. Prediction Model of Dynamic Resilient Modulus of Cohesive Subgrade Soil Based on Triaxial Test System. *Key Eng. Mater.* **2013**, 579–580, 873–876. [[CrossRef](#)]
- Lin, H.; Wang, H.; Fan, X.; Cao, P.; Zhou, K. Particle size distribution effects on deformation properties of graded aggregate base under cyclic loading. *Eur. J. Environ. Civ. Eng.* **2018**. [[CrossRef](#)]
- Zheng, H.; Li, T.; Shen, J.; Xu, C.; Sun, H.; Lü, Q. The effects of blast damage zone thickness on rock slope stability. *Eng. Geol.* **2018**, *246*, 19–27. [[CrossRef](#)]
- Zhang, C.Y.; Pu, C.Z.; Cao, R.H.; Jiang, T.T.; Huang, G. The stability and roof-support optimization of roadways passing through unfavorable geological bodies using advanced detection and monitoring methods, among others, in the Sanmenxia Bauxite Mine in China's Henan Province. *Bull. Eng. Geol. Environ.* **2019**. [[CrossRef](#)]
- Zhao, Y.L.; Zhang, L.Y.; Wang, W.J.; Tang, J.Z.; Lin, H.; Wan, W. Transient pulse test and morphological analysis of single rock fractures. *Int. J. Rock Mech. Min. Sci.* **2017**, *91*, 139–154. [[CrossRef](#)]
- Cao, R.H.; Cao, P.; Lin, H.; Ma, G.; Chen, Y. Failure characteristics of intermittent fissures under a compressive-shear test: Experimental and numerical analyses. *Theor. Appl. Fract. Mech.* **2018**, *96*, 740–757. [[CrossRef](#)]
- Chen, Y.; Lin, H. Consistency analysis of Hoek-Brown and equivalent Mohr-coulomb parameters in calculating slope safety factor. *Bull. Eng. Geol. Environ.* **2018**. [[CrossRef](#)]
- Zhao, Y.L.; Tang, J.Z.; Chen, Y.; Zhang, L.Y.; Wang, W.J.; Liao, J.P. Hydromechanical coupling tests for mechanical and permeability characteristics of fractured limestone in complete stress-strain process. *Environ. Earth Sci.* **2017**, *76*, 1–18. [[CrossRef](#)]
- Zhao, Y.L.; Luo, S.L.; Wang, Y.X.; Wang, W.J.; Zhang, L.Y.; Wan, W. Numerical Analysis of Karst Water Inrush and a Criterion for Establishing the Width of Water-resistant Rock Pillars. *Mine Water Environ.* **2017**, *36*, 508–519. [[CrossRef](#)]
- Zhao, Y.L.; Zhang, L.Y.; Wang, W.J.; Pu, C.Z.; Wan, W.; Tang, J.Z. Cracking and Stress-Strain Behavior of Rock-Like Material Containing Two Flaws Under Uniaxial Compression. *Rock Mech. Rock Eng.* **2016**, *49*, 2665–2687. [[CrossRef](#)]

16. Zhao, Y.L.; Wang, Y.X.; Wang, W.J.; Wan, W.; Tang, J.Z. Modeling of non-linear rheological behavior of hard rock using triaxial rheological experiment. *Int. J. Rock Mech. Min. Sci.* **2017**, *93*, 66–75. [[CrossRef](#)]
17. Fan, X.; Lin, H.; Lai, H.P.; Cao, R.H.; Liu, J. Numerical analysis of the compressive and shear failure behavior of rock containing multi-intermittent joints. *C. R. Méc.* **2019**, *347*, 33–48. [[CrossRef](#)]
18. Wang, Y.X.; Guo, P.P.; Li, X.; Lin, H.; Liu, Y.; Yuan, H.P. Behavior of Fiber-Reinforced and Lime-Stabilized Clayey Soil in Triaxial Tests. *Appl. Sci.* **2019**, *9*, 900. [[CrossRef](#)]
19. Fan, X.; Li, K.H.; Lai, H.P.; Xie, Y.L.; Cao, R.H. Internal stress distribution and cracking around flaws and openings of rock block under uniaxial compression: A particle mechanics approach. *Comput. Geotech.* **2018**, *102*, 28–38. [[CrossRef](#)]
20. Zhou, J.; Li, X.; Mitri, H.S. Evaluation method of rockburst: State-of-the-art literature review. *Tunn. Undergr. Space Technol.* **2018**, *81*, 632–659. [[CrossRef](#)]
21. Wang, Y.X.; Guo, P.P.; Ren, W.X.; Yuan, B.X.; Yuan, H.P.; Zhao, Y.L.; Shan, S.B.; Cao, P. Laboratory Investigation on Strength Characteristics of Expansive Soil Treated with Jute Fiber Reinforcement. *Int. J. Geomech.* **2017**, *17*, 04017101. [[CrossRef](#)]
22. Wang, Y.X.; Guo, P.P.; Dai, F.; Li, X.; Zhao, Y.L.; Liu, Y. Behavior and modeling of fiber-reinforced clay under triaxial compression by combining the superposition method with the energy-based homogenization technique. *Int. J. Geomech.* **2018**, *18*, 04018172. [[CrossRef](#)]
23. Liu, B.C.; Li, C.J.; Pan, Z.Y.; Zhang, B.H. Laboratory test for mechanical properties of Guilin red clay mixed with cement. *J. Eng. Geol.* **2012**, *20*, 633–638.
24. Wang, D.; Wang, H.; Jiang, Y. Water immersion-induced strength performance of solidified soils with reactive MgO—A green and low carbon binder. *J. Test. Eval. (ASTM)* **2019**, *47*. [[CrossRef](#)]
25. Lin, H.; Xiong, W.; Cao, P. Stability of soil nailed slope using strength reduction method. *Eur. J. Environ. Civ. Eng.* **2013**, *17*, 872–885. [[CrossRef](#)]
26. Tan, Y.Z.; Zheng, A.; Wu, P.; Fu, W. Effect of aggregate soil size on California bearing ratio values of laterite soil. *Rock Soil Mech.* **2013**, *34*, 1242–1246.
27. Wang, D.; Du, Y.; Xiao, J. Shear properties of stabilized loess using novel reactive magnesia-bearing binders. *J. Mater. Civ. Eng. (ASCE)* **2019**. [[CrossRef](#)]
28. Meng, J.; Cao, P.; Huang, J.; Lin, H.; Chen, Y.; Cao, R. Second-order cone programming formulation of discontinuous deformation analysis. *Int. J. Numer. Methods Eng.* **2019**, 1–15. [[CrossRef](#)]
29. Wang, H.; Nie, W.; Cheng, W.M.; Liu, Q.; Jin, H. Effects of air volume ratio parameters on air curtain dust suppression in a rock tunnel's fully-mechanized working face. *Adv. Powder Technol.* **2018**, *29*, 230–244. [[CrossRef](#)]
30. Seed, H.B.; Chan, C.K.; Lee, C.E. Resilience characteristics of subgrade soils and their relation to fatigue failures in asphalt pavements. In Proceedings of the International Conference on Structural Design of Asphalt Pavement, Ann Arbor, MI, USA, 20–24 August 1962; pp. 611–636.
31. Ba, M.; Fall, M.; Samb, F.; Sarr, D.; Ndiaye, M. Resilient Modulus of Unbound Aggregate Base Courses from Senegal (West Africa). *Open J. Civ. Eng.* **2011**, *1*, 1–6. [[CrossRef](#)]
32. AASHTO. *Guide for Design of Pavement Structures*; American Association of State Highway and Transportation Officials: Washington, DC, USA, 2002.
33. Shen, J.; Wan, L.; Zuo, J. Non-linear shear strength model for Coal Rocks. *Rock Mech. Rock Eng.* **2019**. [[CrossRef](#)]
34. Huang, F.; Shen, J.; Cai, M.; Xu, C. An empirical UCS model for anisotropic blocky rock masses. *Rock Mech. Rock Eng.* **2019**. [[CrossRef](#)]
35. Shen, J.; Jimenez, R. Predicting the shear strength parameters of sandstone using genetic programming. *B Eng. Geol. Environ.* **2018**, *77*, 1647–1662. [[CrossRef](#)]
36. Seed, H.B.; Mitry, F.G.; Monismith, C.L.; Chan, C.K. *Prediction of Flexible Pavement Deflections from Laboratory Repeated Load Tests*; National Academy of Sciences National Academy of Engineering: Washington, DC, USA, 1967.
37. Uzan, J. *Characterization of Granular Materials*; Transportation Research Record 1022; National Research Council: Washington, DC, USA, 1985; pp. 52–59.
38. Witczak, M.; Uzan, J. *The Universal Airport Design System, Report I of IV. Granular Material Characterization*; University of Maryland: College Park, MD, USA, 1988.

39. Uzan, J. *Characterization of Clayey Subgrade Materials for Mechanistic Design of Flexible Pavements*; Transportation Research Record 1629; Transportation Research Board: Washington, DC, USA, 1998; pp. 188–196.
40. Andrei, D. Development of a Harmonized Test Protocol for the Resilient Modulus of Unbound Materials Used in Pavement Design. Master's Thesis, University of Maryland, College Park, MD, USA, 1999.
41. Ni, B.; Hopkins, T.C.; Sun, L.; Beckham, T.L. Modeling the resilient modulus of soils. In Proceedings of the 6th International Conference on the Bearing Capacity of Roads, Railways and Airfields, Lisbon, Portugal, 24–26 June 2002; pp. 1131–1142.
42. Ozel, M.R.; Mohajerani, A. Resilient Modulus of a Stabilised Fine-grained Subgrade Soil. *Aust. Geomech. J.* **2011**, *36*, 75–86.
43. Li, Z.Y.; Zou, J.R.; Dong, C. Study on Prediction Model of Dynamic Resilient Modulus of Cohesive Subgrade Soils Considering Moisture Variation. *Appl. Mech. Mater.* **2014**, *488–489*, 411–416. [[CrossRef](#)]
44. Bao, T.N.; Mohajerani, A. Resilient Modulus of Fine-grained Soil and a Simple Testing and Calculation Method for Determining an Average Resilient Modulus Value for Pavement Design. *Transp. Geotech.* **2016**, *7*, 59–70.
45. Wang, H.; Lin, H.; Cao, P. Correlation of UCS Rating with Schmidt Hammer Surface Hardness for Rock Mass Classification. *Rock Mech. Rock Eng.* **2017**, *50*, 195–203. [[CrossRef](#)]
46. Liu, Q.; Nie, W.; Yun, H.; Peng, H.T.; Liu, C.Q.; Wei, C.H. Research on tunnel ventilation systems: Dust diffusion and pollution behavior by air curtains based on CFD technology and field measurement. *Build. Environ.* **2019**, *147*, 444–460. [[CrossRef](#)]
47. Hua, Y.; Nie, W.; Cai, P.; Liu, Y.H.; Peng, H.T.; Liu, Q. Pattern characterization concerning spatial and temporal evolution of dust pollution associated with two typical ventilation methods at fully mechanized excavation faces in rock tunnels. *Powder Technol.* **2018**, *334*, 117–131. [[CrossRef](#)]
48. Wang, Y.X.; Guo, P.P.; Lin, H.; Li, X.; Zhao, Y.L.; Yuan, B.X.; Liu, Y.; Cao, P. Numerical Analysis of Fiber-Reinforced Soils based on the Equivalent Additional Stress Concept. *Int. J. Geomech.* **2019**, in press.
49. Chen, R.; Ge, Y.H.; Chen, Z.K.; Liu, J.; Zhao, Y.R.; Li, Z.H. Analytical Solution for One-dimensional Contaminant Diffusion through Unsaturated Soils Beneath. *Geomembrane. J. Hydrol.* **2019**, *568*, 260–274. [[CrossRef](#)]
50. Chen, R.; Huang, J.W.; Chen, Z.K.; Xu, Y.; Liu, J.; Ge, Y.H. Effect of Root Density of Wheat and Okra on Hydraulic Properties of an Unsaturated Compacted Loam. *Eur. J. Soil Sci.* **2019**. [[CrossRef](#)]
51. Lu, M.M.; Jing, H.W.; Zhou, A.N.; Xie, K.H. Analytical models for consolidation of combined composite ground improved by impervious columns and vertical drains. *Int. J. Numer. Anal. Methods Geomech.* **2018**, *42*, 871–888. [[CrossRef](#)]
52. Lu, M.M.; Sloan, S.W.; Indraratna, B.; Jing, H.W.; Xie, K.H. A new analytical model for consolidation with multiple vertical drains. *Int. J. Numer. Anal. Methods Geomech.* **2016**, *40*, 1623–1640. [[CrossRef](#)]
53. Yang, S.B.; Nie, W.; Lv, S.S.; Liu, Z.Q.; Peng, H.T.; Ma, X.; Cai, P.; Xu, C.W. Effects of spraying pressure and installation angle of nozzles on atomization characteristics of external spraying system at a fully-mechanized mining face. *Powder Technol.* **2019**, *343*, 754–764. [[CrossRef](#)]
54. Lu, M.M.; Jing, H.W.; Zhou, Y.; Xie, K.H. General analytical model for consolidation of stone columns-reinforced ground and combined composite ground. *Int. J. Geomechan. (ASCE)* **2017**, *17*, 04016131. [[CrossRef](#)]
55. Cai, P.; Nie, W.; Chen, D.W.; Yang, S.B.; Liu, Z.Q. Effect of air flowrate on pollutant dispersion pattern of coal dust particles at fully mechanized mining face based on numerical simulation. *Fuel* **2019**, *239*, 623–635. [[CrossRef](#)]
56. Bao, Q.; Nie, W.; Liu, C.Q.; Liu, Y.H.; Zhang, H.H.; Wang, H.K.; Jin, H. Preparation and Characterization of a Binary-Graft-Based, Water-Absorbing Dust Suppressant for Coal Transportation. *J. Appl. Polym. Sci.* **2019**, *135*. [[CrossRef](#)]
57. Jin, H.; Nie, W.; Zhang, H.H.; Liu, Y.H.; Bao, Q.; Wang, H.K. The Preparation and Characterization of a Novel Environmentally-Friendly Coal Dust Suppressant. *J. Appl. Polym. Sci.* **2019**. [[CrossRef](#)]
58. Wang, Y.X.; Shan, S.B.; Zhang, C.S.; Guo, P.P. Seismic response of tunnel lining structure in a thick expansive soil stratum. *Tunn. Undergr. Space Technol.* **2019**, *88*, 250–259. [[CrossRef](#)]
59. Yuan, B.X.; Sun, M.; Wang, Y.X.; Zhai, L.H.; Luo, Q.Z. A full 3D displacement measuring system for 3D displacement field of soil around a laterally loaded pile in transparent soil. *Int. J. Geomech.* **2019**. [[CrossRef](#)]

60. Yuan, B.X.; Xu, K.; Wang, Y.X.; Chen, R.; Luo, Q.Z. Investigation of deflection of a laterally loaded pile and soil deformation using the PIV technique. *Int. J. Geomech.* **2017**, *17*, 04016138. [[CrossRef](#)]
61. Wang, D.; Wang, H.; Di, S. Mechanical properties and microstructure of magnesia-fly ash pastes. *Road Mater. Pavement Des.* **2019**. [[CrossRef](#)]
62. Wang, D.; Zentar, R.; Abriak, N.E. Durability and swelling of solidified/stabilized dredged marine soils with class F fly ash, cement and lime. *J. Mater. Civ. Eng. (ASCE)* **2018**, *30*, 04018013. [[CrossRef](#)]
63. Wang, D.; Zentar, R.; Abriak, N.E.; Di, S.J. Long-term mechanical performance of marine sediments solidified with cement, lime and fly ash. *Mar. Georesour. Geotechnol.* **2018**, *36*, 123–130. [[CrossRef](#)]
64. Wang, M.; Shi, X.; Zhou, J.; Qiu, X. Multi-planar detection optimization algorithm for the interval charging structure of large-diameter long hole blasting design based on rock fragmentation aspects. *Eng. Optim.* **2018**, *50*, 2177–2191. [[CrossRef](#)]
65. Peng, H.; Nie, W.; Cai, P.; Liu, Q.; Liu, Z.Q. Development of a novel wind-assisted centralized spraying dedusting device for dust suppression in a fully mechanized mining face. *Environ. Sci. Pollut. Res.* **2018**, 1–16. [[CrossRef](#)]
66. Cao, R.; Cao, P.; Lin, H.; Fan, X.; Zhang, C.; Liu, T. Crack Initiation, Propagation, and Failure Characteristics of Jointed Rock or Rock-Like Specimens: A Review. *Adv. Civ. Eng.* **2019**, *2019*, 6975751. [[CrossRef](#)]
67. Liu, Z.Q.; Nie, W.; Peng, H.T.; Yang, S.B.; Chen, D.W.; Liu, Q. The effects of the spraying pressure and nozzle orifice diameter on the atomizing rules and dust suppression performances of an external spraying system in a fully-mechanized excavation face. *Powder Technol.* **2019**, in press.
68. Lekarp, F.; Isacsson, U.; Dawson, A. Resilient Response of Unbound Aggregates. *J. Transp. Eng.* **2000**, *126*, 66–75. [[CrossRef](#)]
69. Hopkins, T.C.; Beckham, T.L.; Sun, C. *Resilient Modulus of Compacted Crushed Stone Aggregate Bases*; Research Report KTC-05-27/SPR-229-01-1F; Kentucky Transportation Center, College of Engineering, University of Kentucky: Lexington, KY, USA, 2001; p. 89.
70. Ba, M.; Fall, M.; Sall, O.A.; Samb, F. Effect of Compaction Moisture Content on the Resilient Modulus of Unbound Aggregates from Senegal (west Africa). *Geomaterials* **2012**, *2*, 19–23. [[CrossRef](#)]
71. May, R.W.; Witczak, M.W. *Effective Granular Modulus to Model Pavement Response*; Transportation Research Record 810; Transportation Research Board: Washington, DC, USA, 1981; pp. 1–9.
72. Lu, M.M.; Li, D.X.; Jing, H.W.; Deng, Y.B. Analytical solution for consolidation of band-shaped drain based on an equivalent annular drain. *Int. J. Geomech.* **2019**. [[CrossRef](#)]
73. Butterfield, R. Dimensional analysis for geotechnical engineers. *Geotechnique* **1999**, *49*, 357–366. [[CrossRef](#)]



© 2019 by the authors. Licensee MDPI, Basel, Switzerland. This article is an open access article distributed under the terms and conditions of the Creative Commons Attribution (CC BY) license (<http://creativecommons.org/licenses/by/4.0/>).